ARTICLES

Journal of Semiconductors
(2023) 44, 032501
doi: 10.1088/1674-4926/44/3/032501

Colossal negative magnetoresistance in spin glass Na(Zn,Mn)Sb

Shuang Yu[1, 2], Yi Peng[1, 2], Guoqiang Zhao[1, 2], Jianfa Zhao[1, 2], Xiancheng Wang[1, 2], Jun Zhang[1, 2], Zheng Deng[1, 2, †], and Changqing Jin[1, 2, †]

[1]Beijing National Laboratory for Condensed Matter Physics, and Institute of Physics, Chinese Academy of Sciences, Beijing 100190, China
[2]School of Physics, University of Chinese Academy of Sciences, Beijing 100190, China

Abstract: We report the study of magnetic and transport properties of polycrystalline and single crystal Na(Zn,Mn)Sb, a new member of "111" type of diluted magnetic materials. The material crystallizes into Cu_2Sb-type structure which is isostructural to "111" type Fe-based superconductors. With suitable carrier and spin doping, the Na(Zn,Mn)Sb establishes spin-glass ordering with freezing temperature (T_f) below 15 K. Despite lack of long-range ferromagnetic ordering, Na(Zn,Mn)Sb single crystal still shows sizeable anomalous Hall effect below T_f. Carrier concentration determined by Hall effect measurements is over 10^{19} cm^{-3}. More significantly, we observe colossal negative magnetoresistance (MR $\equiv [\rho(H) - \rho(0)]/\rho(0)$) of –94% in the single crystal sample.

Key words: colossal negative magnetoresistance; spin glass; diluted magnetic materials

Citation: S Yu, Y Peng, G Q Zhao, J F Zhao, X C Wang, J Zhang, Z Deng, and C Q Jin, Colossal negative magnetoresistance in spin glass Na(Zn,Mn)Sb[J]. *J. Semicond.*, 2023, 44(3), 032501. https://doi.org/10.1088/1674-4926/44/3/032501

1. Introduction

Tunable ferromagnetism is one of the most exotic properties in diluted magnetic materials of which local spins are meditated by carriers[1–5]. Thus transport behaviors have been one of the prominent aspects in the studies of diluted magnetic materials. Particularly, magnetoresistance (MR) effect in diluted magnetic semiconductors (DMS) has been studied for decades for its diversified physical mechanisms and potential application on spintronic circuits[6]. Diluted magnetic alloys, such as spin-glassy AuFe, AuMn usually exhibit negative MR ratios of only several percentages[7]. For II–IV based DMSs with low carrier concentration (~10^{17} cm^{-3}), n-type (Cd,Mn)Se and p-type (Hg,Mn)Te show pronounced negative MR[8]. On the other hand, classical III–V based ferromagnetic (FM) DMS (Ga,Mn)As has negative MR of about 10%–30%[9].

Recently, a serious of new types of DMS with independent carrier and spin doping were discovered[10–15]. Among these new materials, an exciting high Curie temperature of 230 K was reached in the so called "122" DMS $(Ba,K)(Zn,Mn)_2As_2$[16]; large MR were found in polycrystalline $(Sr,K)(Zn,Mn)_2As_2$ and $(Ba,K)(Cd,Mn)_2As_2$[17, 18]. These features inspired further experimental and theoretical investigations on these new types of DMS[19–21]. Interestingly, most of them are isostructural to corresponding Fe-based superconductors, which are composed of one FeAs layer sandwiched by two charge layers, offering intriguing possibilities to fabricate and study multilayer isostructure-hetrojuctions[13, 22–24].

The "111" DMS, Li(Zn,Mn)As and Li(Zn,Mn)P, crystalize into zinc-blende like structure[10, 25]. The related compounds NaZnX (X = P, As and Sb) are found to crystallize in the tetragonal Cu_2Sb-type structure. Most of new types of DMS are based on arsenide compounds, while antimonide based materials are less investigated. Thus in the present work, we focus on the synthesis and characterization of the excess-Na and Mn doped Na(Zn,Mn)Sb. Although the parent phase NaZnSb is a gapless metal, its carrier concentration is only 10^{18} cm^{-3}[26]. Excess-Na doping increases the carrier concentration to 4×10^{19} cm^{-3}. Together with Mn-doping, spin-glass (SG) state is found in Na(Zn,Mn)Sb. Despite of short-range ordering, we still observe colossal negative MR in single crystal samples of Na(Zn,Mn)Sb.

2. Experiments

Polycrystalline specimens of $Na_{1+x}(Zn_{1-y}Mn_y)Sb$ were synthesized by solid state[10, 11]. Single crystal samples were grown by self-flux method[13]. The real atom ratio of the single crystals was determined by energy dispersive X-ray analysis (EDX).

The crystal structure of the polycrystalline and single-crystal specimens was characterized by X-ray diffraction (XRD) using a Philips X'pert diffractometer at room temperature. Rietveld refinements were performed with GSAS software packages to obtain lattice parameters[27]. DC magnetic susceptibility was measured between 2 and 300 K with a superconducting quantum interference device (SQUID) magnetometer. A physical properties measurement system (PPMS) was used for AC magnetic susceptibility and electrical transport measurements. Resistivity measurements were conducted with the four-probe method, and Hall effect was measured with standard Hall bar contact.

3. Results and discussion

The XRD patterns and crystal structure of Na(Zn,Mn)Sb are shown in Fig. 1. In Fig. 1(a) all the peaks of the polycrystalline $Na_{1.1}(Zn_{1-y}Mn_y)Sb$ ($0.05 \leqslant y \leqslant 0.40$) can be indexed with a Cu_2Sb-type structure (space group *P4/nmm*). Fig. 1(b)

Correspondence to: Z Deng, dengzheng@iphy.ac.cn; C Q Jin, Jin@iphy.ac.cn
Received 30 SEPTEMBER 2022; Revised 28 OCTOBER 2022.

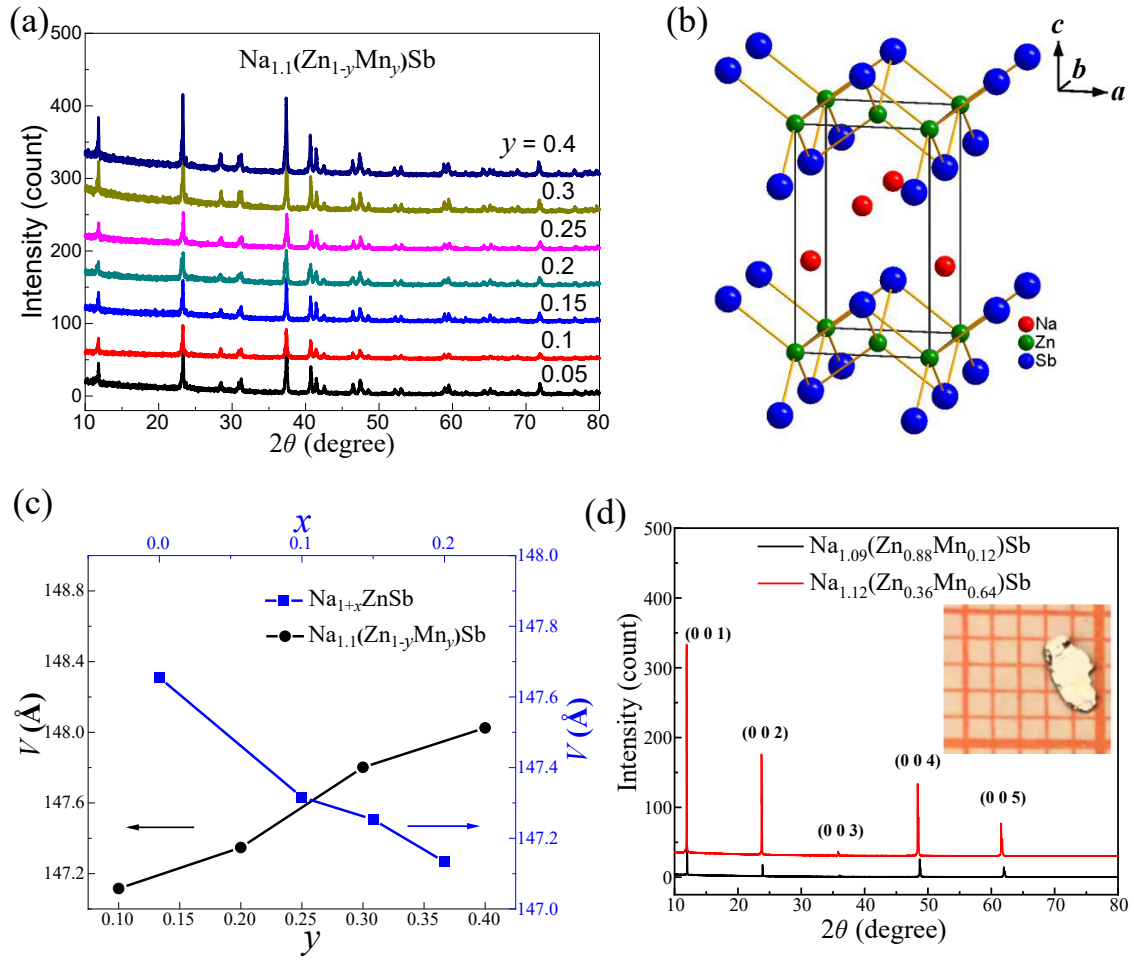

Fig. 1. (Color online) (a) XRD patterns of $Na_{1.1}(Zn_{1-y}Mn_y)Sb$ ($0.05 \leqslant y \leqslant 0.40$). (b) Crystal structure of Na(Zn,Mn)Sb. (c) Cell volume of $Na_{1+x}(Zn_{1-y}Mn_y)Sb$ for various doping concentrations of Na and Mn. (d) XRD patterns of single crystal $Na_{1.09}(Zn_{0.88}Mn_{0.12})Sb$ and $Na_{1.12}(Zn_{0.36}Mn_{0.64})Sb$.

shows the crystal structure of Na(Zn,Mn)Sb where $(Zn,Mn)Sb_4$ tetrahedra form square *a*-*b* planes and Na layers separate (Zn,Mn)Sb layers along *c*-axis. The volume of unit cell decreases with increasing Na, while Mn-doping increases the volume of unit cell (Fig. 1(c)). The changes of cell volume suggest successful chemical doping of Na and Mn. The real atom ratio of the single crystals with two nominalcompositions $Na_{1.1}(Zn_{0.9}Mn_{0.1})Sb$ and $Na_{1.1}(Zn_{0.4}Mn_{0.6})As$ are $Na_{1.09}Zn_{0.88}Mn_{0.12}Sb$ and $Na_{1.12}Zn_{0.36}Mn_{0.64}Sb$ respectively. The inset of Fig. 1(d) shows a typical piece of single crystal with dimensions of $3 \times 2 \times 0.25$ mm^3. The XRD patterns of $Na_{1.09}Zn_{0.88}Mn_{0.12}Sb$ and $Na_{1.12}Zn_{0.36}Mn_{0.64}Sb$ are shown in Fig. 1(d). Only peaks of (00l) appear, indicating the surfaces of the single crystals are perpendicular to the crystallographic *c*-axis.

For varying Na concentrations of $Na_{1+x}(Zn_{1-y}Mn_y)Sb$, the samples with $x = 0.1$, i.e., $Na_{1.1}(Zn_{1-y}Mn_y)Sb$, have most distinct magnetic transition. Thus we focus our discussion on the sample $Na_{1.1}(Zn_{1-y}Mn_y)Sb$ in the following text. Temperature-dependence of DC magnetization, ($M(T)$) for polycrystalline samples with $0.05 \leqslant y \leqslant 0.4$ are plotted in Fig. 2(a), where samples with low Mn concentrations ($y = 0.05$ and 0.1) don't show visible magnetic transition down to 2 K. For samples with more Mn, upturns appear on both ZFC and FC curves at about 12–15 K. On lowing temperature, "λ"-shape divergences between ZFC and FC can be found, which resemble spin-glass like transitions. For $y \leqslant 0.3$, the irreversible temperatures (T_{irr}) and the maximum points on ZFC (T_s) increase from 8.6 to 12.9 K and 7.0 to 12.0 K with increasing Mn doping levels respectively. When y increases to 0.4, T_{irr} and T_s decrease to 9.7 and 10.0 K respectively. Fig. 2(b) shows field-dependence of magnetization ($M(H)$) where "S"-sharp curves also indicate spin-glass like states of magnetic moments. The open loops, which are sign of existence of FM component, are only visible in the sample with $y > 0.1$. Magnetic anisotropy of single crystal $Na_{1.12}Zn_{0.36}Mn_{0.64}Sb$ is shown in Fig. 2(c) where out-of-plane ($H//c$) magnetization is larger than in-plane ($H//ab$) magnetization in both $M(T)$ and $M(H)$ curves. The open out-of-plane hysteresis loop demonstrates FM component along *c*-axis.

It is noteworthy that the magnetic signal indeed shows a non-monoclinic change with Mn doping levels (Figs. 2(a) and 2(b)). It firstly increases at lower Mn doping levels and then decreases at higher Mn concentrations. The magnetic signal is basically from spin glass ordering, which is generated by magnetic frustration. Generally, there are ferromagnetic and antiferromagnetic interactions in a diluted magnetic material. In Na(Zn,Mn)Sb, the former is carrier-mediated between two distanced Mn^{2+}, and the latter is short range between neighbor Mn^{2+}. When Mn concentration is low, neighbor Mn are relatively rare. Thus, ferromagnetic and antiferromagnetic interactions are comparable and spin glass ordering can be en-

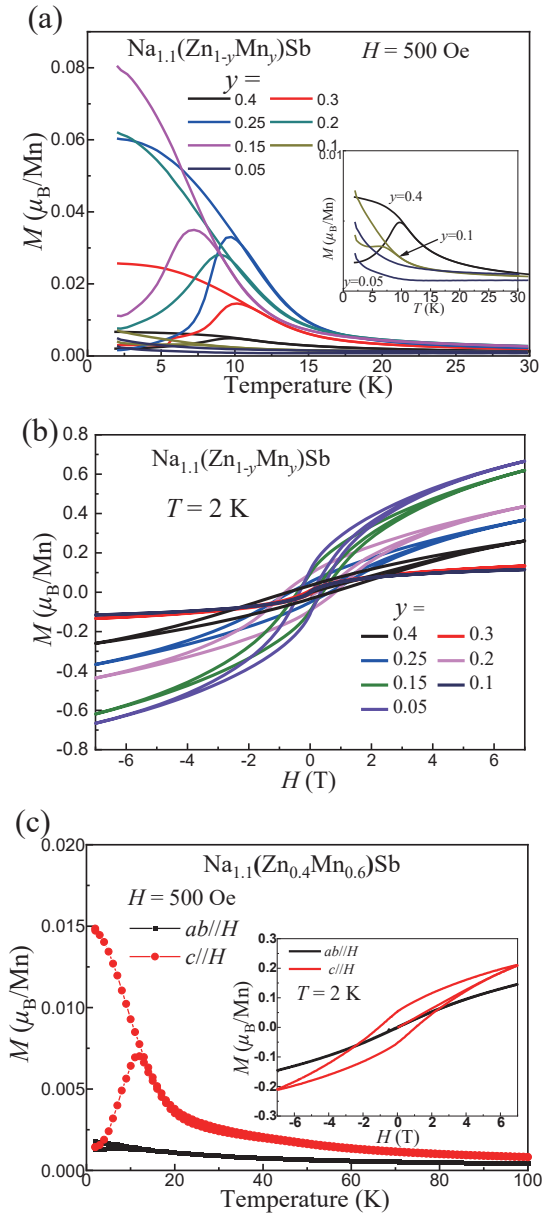

Fig. 2. (Color online) (a) The DC magnetization measured in $Na_{1.1}(Zn_{1-y}Mn_y)Sb$, ($0.05 \leqslant y \leqslant 0.4$) in $H = 500$ Oe with ZFC and FC procedures. (b) $M(H)$ curves measured at 2 K for $Na_{1.1}(Zn_{1-y}Mn_y)Sb$. (c) $M(T)$ and $M(H)$ curves for single crystal $Na_{1.12}(Zn_{0.36}Mn_{0.64})Sb$.

hanced with increasing Mn. However, when Mn concentration is high, neighbor Mn dominate the lattice. Thus, antiferromagnetic interaction is predominating, and one can find that spin glass ordering is suppressed by further Mn-doping.

To confirm the spin-glass behaviors, AC susceptibility measurements were performed. As a typical example, Fig. 3(a) shows the results of AC susceptibility under zero field of different frequencies f with amplitude of H = 10 Oe for $Na_{1.1}(Zn_{0.75}Mn_{0.25})Sb$. Both of the real part (χ') and imaginary part (χ'') show frequencies-dependence, a hallmark of magnetic glassy state. The peaks on the real part $\chi'(T)$ (freezing temperature, T_f) and $\chi''(T)$ shift to higher temperatures with increasing frequencies. This frequency dependence of T_f (Eq. (1)) is usually characterized by the term[28],

$$K = \Delta T_f/[T_f(\Delta \log f)]. \quad (1)$$

We obtained K = 0.033 which is in the range 0.004–0.08 for spin-glass systems. Another way to characterize spin-glass behavior is to fit T_f dependence of f with critical slowing down relation (Eq. (2))[29],

$$\frac{\tau}{\tau_0} = \left(\frac{T_f - T_0}{T_0}\right)^{-z\nu}, \quad (2)$$

where τ_0 is the characteristic relaxation time of single spin flip, $\tau = 1/f$, T_0 is underlying spin-glass transition temperature determined by the interactions in the system, z is the dynamic critical exponent, and ν is the critical exponent of the correlation length. The best fitting parameters obtained for polycrystalline $Na_{1.1}(Zn_{0.75}Mn_{0.25})Sb$ are T_0 = 11.52 K, $\tau_0 = 10^{-10}$ s, and $z\nu$ = 7.3. The values expected for canonical spin-glassed are $\tau_0 = 10^{-10}$–10^{-12} s and $z\nu$ = 5–10. The obtained parameters are in the range of typical spin-glasses (Fig. 3(b)). For polycrystalline $Na_{1.1}(Zn_{0.6}Mn_{0.4})Sb$ the obtained parameters are K = 0.056, T_0 = 13.79 K, $\tau_0 = 10^{-8}$, and $z\nu$ = 4.9. The increasing K with the increasing Mn concentration indicates T_f becomes more frequencies-dependent. One can also notice that the parameter K is still within the range of typical spin-glasses but τ_0 doesn't.

Fig. 4(a) shows resistivity dependence of temperature ($\rho(T)$) of the parent phase, polycrystalline NaZnSb. The metallic behavior is consistent with previous report[26]. According to Hall effect measurements the majority carrier is hole with nearly constant concentration of 9×10^{18} cm^{-3} at 2 and 50 K (inset of Fig. 4(a)). Excess-Na doping induces extra holes into the material. Fig. 4(b) shows Hall resistivity of single crystal $Na_{1.09}(Zn_{0.88}Mn_{0.12})Sb$ at varying temperatures. At low temperature (10 and 15 K) where short-range ordering forms, it is surprising to find larger anomalous Hall effect (AHE) dominates low field range. Large AHE has also been found in SG-like $Ge_{1-x-y}Sn_xMn_yTe$[30]. The AHE indicates strong spin-orbit coupling and spin polarization[31]. The hole concentrations of single crystal $Na_{1.09}(Zn_{0.88}Mn_{0.12})Sb$ is 3.0×10^{19} cm^{-3} at 100 K, which is over three times larger than that of parent phase. The hole concentration of Na(Zn,Mn)Sb is slightly smaller than that of Li(Zn,Mn)As and (Ba,K)$(Zn,Mn)_2As_2$[10, 11].

On the other hand, Mn-doping dramatically increases resistivity of the system, particularly at low temperature. $Na_{1.12}(Zn_{0.36}Mn_{0.64})Sb$ has ρ_{5K} = 6826.5 Ω·mm and ρ_{20K} = 2455.2 Ω·mm while $Na_{1.09}(Zn_{0.88}Mn_{0.12})Sb$ has ρ_{5K} = 9.1 Ω·mm and ρ_{20K} =3.9 Ω·mm. Nevertheless, Mn-doping actually decreases carrier concentration only by relatively small amplitude. The hole concentration of $Na_{1.12}(Zn_{0.36}Mn_{0.64})Sb$ is 1.7×10^{19} cm^{-3} at 100 K which is comparable to that of $Na_{1.09}(Zn_{0.88}Mn_{0.12})Sb$ (3.0×10^{19} cm^{-3} at 100 K). Thus, there must be other factor to increase resistivity in heavy Mn-doping level sample. In a material doped by magnetic element, both disorder-induced localization and magnetic scattering are feasible to reduce mean free path of carriers and in turn to increase resistivity. To clarify the puzzle, a sample with non-magnetic-substitution, Na(Zn,Mg)Sb, was synthesized and characterized. Although only 5% Mg could be doped into Zn site without inducing a second phase, one can still find the distinctly difference between $Na_{1.1}(Zn_{0.95}Mg_{0.05})Sb$ and $Na_{1.1}(Zn_{0.95}Mn_{0.05})Sb$. On lowering temperature, both of the samples show metallic behavior until 30–40 K and then monotonic increases of resistivity. However, amplitude of uprising on $\rho(T)$ of Mn-doped-sample is 5 times larger than that of

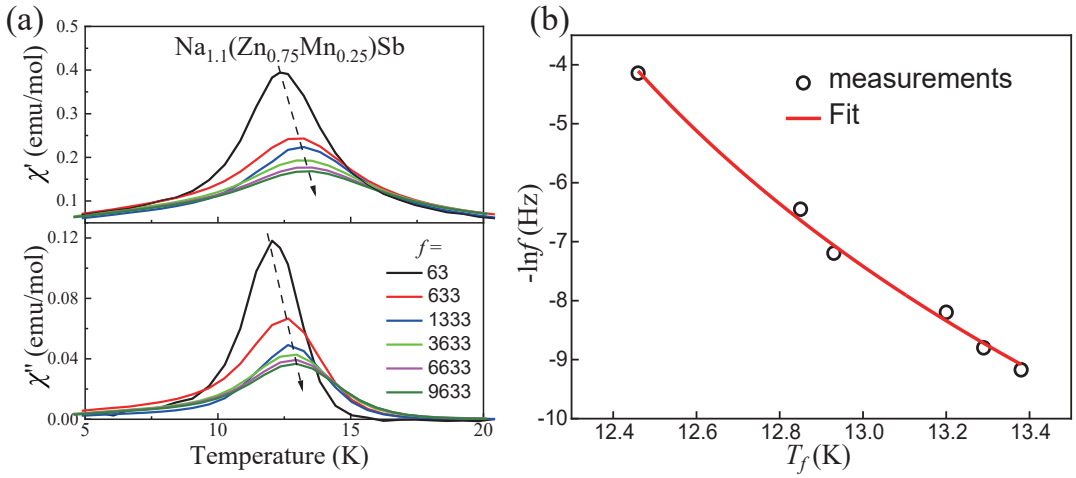

Fig. 3. (Color online) (a) AC χ'(*T*) and χ''(*T*) of $Na_{1.1}(Zn_{0.75}Mn_{0.25})Sb$ at various frequencies. (b) The best fit of T_f data extracted from Fig. 3(a) to the Eq. (2).

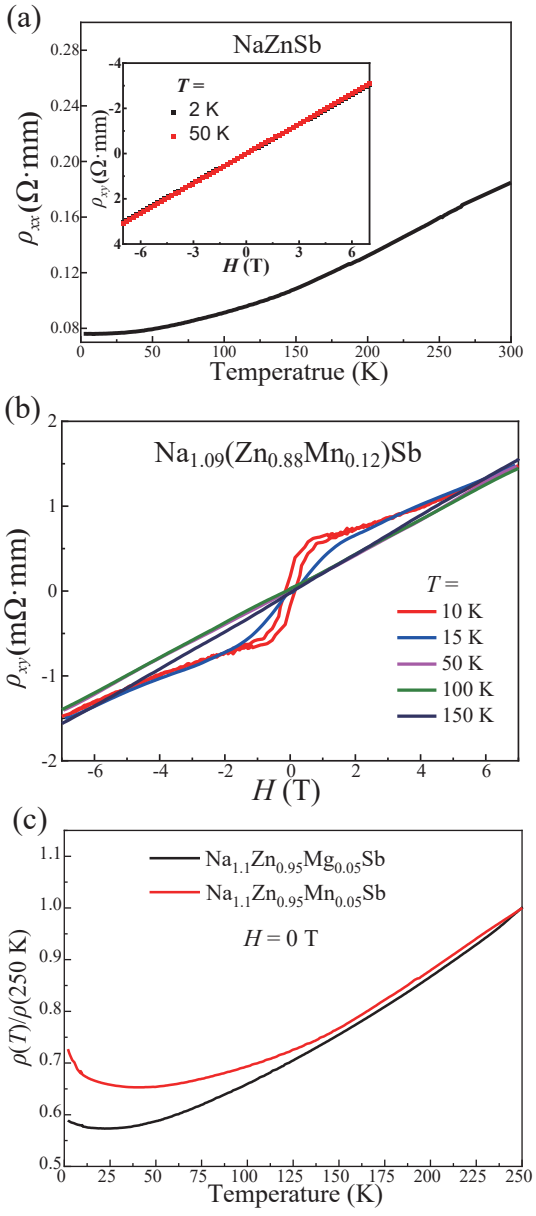

Fig. 4. (Color online) (a) Temperature dependence of resistivity for NaZnSb. The inset shows hall resisitivity for NaZnSb at 2 and 50 K. (b) Hall resisitivity of $Na_{1.09}(Zn_{0.88}Mn_{0.12})Sb$ at various temperature. (c) Temperature dependence of resistivity of $Na_{1.1}(Zn_{0.95}Mg_{0.05})Sb$ and $Na_{1.1}(Zn_{0.95}Mn_{0.05})Sb$. Note that amplitude is normalized.

Mg-one, implying magnetic scattering is a main factor to influence conduction behavior in Na(Zn,Mn)Sb compounds (Fig. 4(c)).

At low temperature, large MR has been observed in both polycrystalline and single crystal samples. For polycrystalline samples without spin glass (SG) transition, MR (MR ≡ [$\rho(H)$ – $\rho(0)$]/$\rho(0)$) are significantly smaller, *e.g.* MR_{2K} = –5% and –13% in $Na_{1.1}Zn_{0.95}Mn_{0.05}Sb$ and $Na_{1.1}Zn_{0.9}Mn_{0.1}Sb$. MR_{2K} dramatically increases to –90% in polycrystalline $Na_{1.1}Zn_{0.85}Mn_{0.15}Sb$ where spin-glass transition occurs at about 5 K. Two single crystal samples also present colossal MR at low temperature. In Fig. 5(a), $\rho(T)$ of single crystal $Na_{1.09}(Zn_{0.88}Mn_{0.12})Sb$ at various applied fields are plotted. The curves diverge at about 15 K where upturn on $M(T)$ appears. The uprising on $\rho(T)$ is completely suppressed by magnetic field at H = 7 T. In Fig. 5(b), $MR_{20K}(H)$ doesn't saturate at 7 T and the maximum value is –24%. On lowering temperature, MR(H) curves gradually saturate and reach larger value with MR_{2K} of –70%. The hysteresis on $MR_{2K}(H)$ is about 1 T, close to the value obtained from $M(H)$. Single crystal $Na_{1.12}(Zn_{0.36}Mn_{0.64})Sb$ shows similar behavior with larger MR_{2K} of –94% (Figs. 5(c)–5(d)).

Different from FM $(Ba_{0.9}K_{0.1})(Cd_{2-x}Mn_x)_2As_2$, $(Sr_{0.9}K_{0.1})$-$(Zn_{1.8}Mn_{0.2})_2As_2$, and GaMnAsP, which also showed colossal negative MR in FM states, Na(Zn,Mn)Sb manifested colossal negative MR in SG states[17, 18, 32]. On the other hand, the striking negative MR in SG (Cd,Mn)Se and (Hg,Mn)Te is associated with *sp-d* exchange effects or bound magnetic polarons[8]. Note that their carrier concentrations are 2 orders lower than tile materials, thus the microscopic models for MR could be completely different. Taking into account the magnetic scattering from Mn, we propose that the negative MR is related with spin scatting declining under external fields. More importantly, in II–VI DMSs isovalent Mn^{2+} doping provides only spin but not carrier. As discussed above, carrier concentration of Na(Zn,Mn)Sb can be tuned by controlling extra Na-doping level. On the other hand, Na(Zn,Mn)Sb is not only isostructural to but also lattice-matched with some functional materials, such as high-temperature Fe-based superconductor NaFeAs and antiferromagnetic NaMnAs. This feature offers possibilities to fabricate and study isostructural heterojunctions composed by various combinations of these materials.

4. Conclusion

In summary, a new diluted magnetic compound

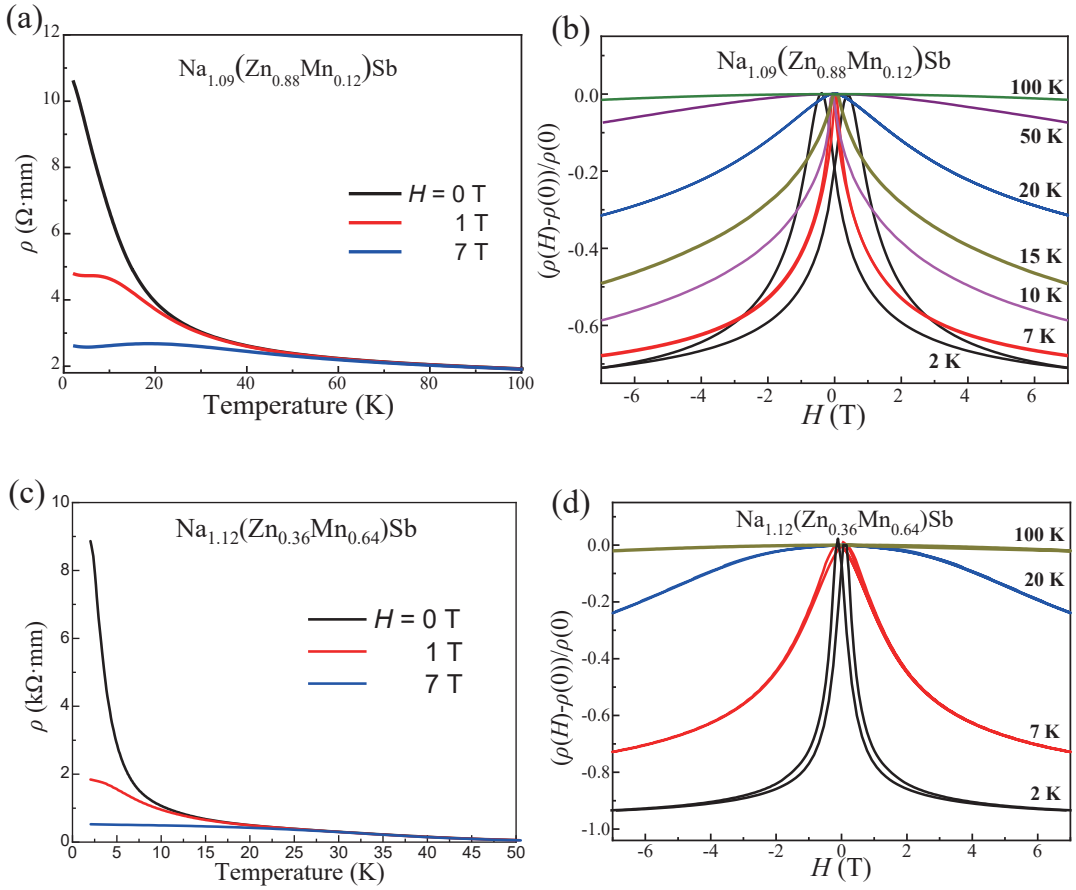

Fig. 5. (Color online) (a) $\rho(T)$ of single crystal $Na_{1.09}(Zn_{0.88}Mn_{0.12})Sb$ at various applied fields. (b) MR(H) curves of single crystal $Na_{1.09}(Zn_{0.88}Mn_{0.12})Sb$ at various temperature. (c) $\rho(T)$ of single crystal $Na_{1.12}(Zn_{0.36}Mn_{0.64})Sb$ at various applied fields. (d) MR(H) curves of single crystal $Na_{1.12}(Zn_{0.36}Mn_{0.64})Sb$ at various temperature.

Na(Zn,Mn)Sb with decoupled charge and spin doping has been synthesized. With co-doped Excess-Na and Mn to induce hole carrier and spin, Na(Zn,Mn)Sb can establish a spin-glass ordering at low temperature. The detailed studies indicate that colossal negative magnetoresistance is related with spin-glass ordering. The maximum value of magnetoresistance of –94% has been found in single crystal sample. The title material extends magnetic states to explore colossal magnetoresistance.

Acknowledgements

This work was financially supported by the Ministry of Science and Technology (MOST), NSF of China through the research projects (2018YFA03057001, 11820101003), and CAS Project for Young Scientists in Basic Research (YSBR-030). Z. Deng acknowledges support of Beijing Nova program (2020133) and the Youth Innovation Promotion Association of CAS (2020007).

References

[1] Žutić I, Fabian J, Das Sarma S. Spintronics: Fundamentals and applications. Rev Mod Phys, 2004, 76, 323

[2] Dietl T, Ohno H, Matsukura F, et al. Zener model description of ferromagnetism in zinc-blende magnetic semiconductors. Science, 2000, 287, 1019

[3] Dietl T. A ten-year perspective on dilute magnetic semiconductors and oxides. Nat Mater, 2010, 9, 965

[4] Hirohata A, Sukegawa H, Yanagihara H, et al. Roadmap for emerging materials for spintronic device applications. IEEE Trans Magn, 2015, 51, 1

[5] Song L, Yan W, Wang H L, et al. Resonant enhancement of magnetic damping driven by coherent acoustic phonons in thin Co_2FeAl film epitaxied on GaAs. J Semicond, 2021, 42, 032501

[6] von Molnár S. Magnetotransport in magnetic semiconductors and possible applications. Sens Actuat A, 2001, 91, 161

[7] Nigam A K, Majumdar A K. Magnetoresistance in canonical spin-glasses. Phys Rev B, 1983, 27, 495

[8] Furdyna J K. Diluted magnetic semiconductors. J Appl Phys, 1988, 64, R29

[9] Paalanen M A, Bhatt R N. Transport and thermodynamic properties across the metal-insulator transition. Phys B, 1991, 169, 223

[10] Deng Z, Jin C Q, Liu Q Q, et al. Li(Zn, Mn)As as a new generation ferromagnet based on a I–II–V semiconductor. Nat Commun, 2011, 2, 422

[11] Zhao K, Deng Z, Wang X C, et al. New diluted ferromagnetic semiconductor with Curie temperature up to 180 K and isostructural to the '122' iron-based superconductors. Nat Commun, 2013, 4, 1442

[12] Zhao G Q, Deng Z, Jin C Q. Advances in new generation diluted magnetic semiconductors with independent spin and charge doping. J Semicond, 2019, 40, 081505

[13] Zhao G Q, Lin C J, Deng Z, et al. Single crystal growth and spin polarization measurements of diluted magnetic semiconductor $(BaK)(ZnMn)_2As_2$. Sci Rep, 2017, 7, 14473

[14] Zhao X, Dong J, Fu L, et al. $(Ba_{1-x}Na_x)F(Zn_{1-x}Mn_x)Sb$: A novel fluoride-antimonide magnetic semiconductor with decoupled charge and spin doping. J Semicond, 2022, 43, 112501

[15] Dong J, Zhao X Q, Fu L C, et al. (Ca, K)(Zn, Mn)$_2As_2$: Ferromagnetic semiconductor induced by decoupled charge and spin doping in $CaZn_2As_2$. J Semicond, 2022, 43, 072501

[16] Zhao K, Chen B J, Zhao G Q, et al. Ferromagnetism at 230 K in $(Ba_{0.7}K_{0.3})(Zn_{0.85}Mn_{0.15})_2As_2$ diluted magnetic semiconductor. Chin Sci Bull, 2014, 59, 2524
[17] Yang X J, Chen Q, Li Y P, et al. $Sr_{0.9}K_{0.1}Zn_{1.8}Mn_{0.2}As_2$: A ferromagnetic semiconductor with colossal magnetoresistance. EPL Europhys Lett, 2014, 107, 67007
[18] Yang X J, Li Y K, Zhang P, et al. K and Mn co-doped $BaCd_2As_2$: A hexagonal structured bulk diluted magnetic semiconductor with large magnetoresistance. J Appl Phys, 2013, 114, 223905
[19] Suzuki H, Zhao K, Shibata G, et al. Photoemission and X-ray absorption studies of the isostructural to Fe-based superconductors diluted magnetic semiconductor $Ba_{1-x}K_x(Zn_{1-y}Mn_y)_2As_2$. Phys Rev B, 2015, 91, 140401
[20] Frandsen B A, Gong Z Z, Terban M W, et al. Local atomic and magnetic structure of dilute magnetic semiconductor (Ba, K)(Zn, Mn)$_2$-As_2. Phys Rev B, 2016, 94, 094102
[21] Glasbrenner J K, Žutić I, Mazin I I. Theory of Mn-doped II-II-V semiconductors. Phys Rev B, 2014, 90, 140403
[22] Žutić I, Zhou T. Tailoring magnetism in semiconductors. Sci China Phys Mech Astron, 2018, 61, 067031
[23] Wang X C, Liu Q Q, Lv Y X, et al. The superconductivity at 18 K in Li-FeAs system. Solid State Commun, 2008, 148, 538
[24] Wang R, Huang Z X, Zhao G Q, et al. Out-of-plane easy-axis in thin films of diluted magnetic semiconductor $Ba_{1-x}K_x(Zn_{1-y}Mn_y)_2As_2$. AIP Adv, 2017, 7, 045017
[25] Deng Z, Zhao K, Gu B, et al. Diluted ferromagnetic semiconductor Li(Zn, Mn)P with decoupled charge and spin doping. Phys Rev B, 2013, 88, 081203
[26] Jaiganesh G, Merita Anto Britto T, Eithiraj R D, et al. Electronic and structural properties of NaZnX (X = P, As, Sb): An *ab initio* study. J Phys: Condens Matter, 2008, 20, 085220
[27] Toby B H. EXPGUI, a graphical user interface for GSAS. J Appl Cryst, 2001, 34, 210
[28] Deng Z, Retuerto M, Liu S Z, et al. Dynamic ferrimagnetic order in a highly distorted double perovskite Y_2CoRuO_6. Chem Mater, 2018, 30, 7047
[29] Dho J, Kim W S, Hur N H. Reentrant spin glass behavior in Cr-doped perovskite manganite. Phys Rev Lett, 2002, 89, 027202
[30] Kilanski L, Szymczak R, Dobrowolski W, et al. Negative magnetoresistance and anomalous Hall effect in GeMnTe-SnMnTe spin-glass-like system. J Appl Phys, 2013, 113, 063702
[31] Sinova J, Jungwirth T, Černe J. Magneto-transport and magneto-optical properties of ferromagnetic (III, Mn)V semiconductors: A review. Int J Mod Phys B, 2004, 18, 1083
[32] Liu X, Riney L, Guerra J, et al. Colossal negative magnetoresistance from hopping in insulating ferromagnetic semiconductors. J Semicond, 2022, 43, 112502

Shuang Yu received her Ph.D. degree from Institute of Physics, Chinese Academy of Sciences in 2020. Since 2015, she has been working in Prof. Changqing Jin's group under the supervision of Associate Professor Zheng Deng and Professor Changqing Jin, with research focusing on magnetic semiconductors. Now she works in Intel Company at Dalian.

Zheng Deng received his Ph.D. degree from Institute of Physics, Chinese Academy of Sciences in 2012. He worked as a postdoc in the Department of Chemistry in Rutgers University from 2013.1 to 2015.1. Since then, he has been working as an associate professor at IOPCAS. His research interests include magnetic semiconductors, superconductors and emergent materials under extreme conditions.

Changqing Jin is currently a professor at Institute of Physics, Chinese Academy of Sciences. He received his Ph.D. degree from IOPCAS in 1991. He is a fellow of American Physical Society, a fellow of American Association for the Advancement of Science, and a fellow of the Institute of Physics (UK). His research group focuses on new Quantum matters by design using extreme conditions, and effects of pressures on novel emergent phenomena.